


## Persistence of ferromagnetic domains in a disordered two-dimensional lattice

C. Madroñero, G. A. Domínguez-Castro, L. A. González-García, and R. Paredes\*

*Instituto de Física, Universidad Nacional Autónoma de México, Apartado Postal 20-364, México Distrito Federal 01000, Mexico*

 (Received 27 January 2020; revised 30 June 2020; accepted 6 August 2020; published 2 September 2020)

We investigate the persistence, in time and space, of ferromagnetic domains in two dimensions subjected to the influence of both the static disorder of variable strength and weak interactions. The domains are represented by a two-species bosonic mixture of  $^{87}\text{Rb}$  ultracold atoms in different hyperfine states, such that initially one lies on the left half and the other on the right half of a square lattice. The dynamics of the double domain is followed by describing the two-component superfluid through the time-dependent Gross-Pitaevskii coupled equations, with values of the intra- and interspecies interaction that guarantee miscibility of the components. A robust analysis of the magnetization dynamics for several values of the interspecies interaction, reachable in current experimental setups, and the investigation of the density-weighted magnetization correlator lead us to conclude that the presence of structural disorder yields a slowdown the process of destruction of the initial ferromagnetic order. As shown by our numerical calculations, magnetization is maintained up to 50% of its initial value for the largest disorder amplitude considered.

DOI: [10.1103/PhysRevA.102.033304](https://doi.org/10.1103/PhysRevA.102.033304)

### I. INTRODUCTION

A vast number of phenomena belonging to condensed matter remain until now unsolved. In particular, within the magnetism realm, the dynamics of microscopic spins lying in ultrathin films, the so-called magnetic domain dynamics, continue until now as an open question [1–3]. The origin of the spin-domain dynamics can be attributed to several factors, among them, the presence of external drivings as magnetic or electric fields, the existence of spin-polarized currents inducing the transference of momentum to the domain wall [4,5], and the inner dynamics associated with both the interactions between the microscopic constituents and the energetic landscape where the constituents move. The purpose of the present investigation is to analyze the dynamics of the magnetic domains confined in two dimensions (2D) under the influence of disorder. As we describe in the next paragraph, a stylized system is used to address this objective.

Inspired by the remarkable control achieved with large conglomerates of atoms in their quantum degenerate state, and in particular by the experimental capacity of preparing mixtures composed of either Bose condensates in different hyperfine states [6] or different atomic species [7–11], confined in particular geometries [12–16], we propose here the design of an *ultracold atom device* to quantum simulate the decay of magnetization in magnetic domains in 2D square lattices subjected to static disorder. Our proposal is based on previous experiments that explore the many-body localization phenomenon with  $^{87}\text{Rb}$  Bose gases [17,18]. In particular, in Ref. [17] the dynamics of an initially prepared out-of-equilibrium density pattern confined in a disordered optical lattice was followed. Such a quantum quench protocol, planned to

track the effects of disorder on the atom flux moving across the two-dimensional (2D) lattice, together with the possibility of spatially separating different hyperfine components, is the basis of our proposal to study the dynamics of the ferromagnetic domains, particularly their magnetization decay.

To investigate the dynamics of the ferromagnetic domains, and particularly their magnetization decay, we consider a two-species Bose condensate as the analog of a double-spin domain in which each hyperfine component lies in the halves of an inhomogeneous square lattice, thus setting the initial configuration that will evolve in a disordered media (see Fig. 1). This arrangement together with a recent study, performed at the mean-field level for the stationary states of a scalar Bose condensate [19], is our starting point to study the dynamics of the double-spin domain. Although the present study considers square lattices only, investigation of other geometrical configurations, like those considered in Ref. [19], could be of interest in the light of practical purposes such as the design of spin-based magnetic protocols with complex configurations.

Here we present the results of an extensive set of numerical calculations performed at the mean-field level through the coupled Gross-Pitaevskii (GP) equations to describe the evolution in time of the hyperfine spin components spatially separated at  $t = 0$  and then allowed to evolve under the influence of uncorrelated static disorder. Working within the superfluid regime, corresponding to values of the intraspecies interaction such that the system is far from the Mott-insulating phases, we analyze the evolution of the magnetization for a given initial state, considering different values of the ratio between intra- and interspecies interaction strengths. Motivated by the analysis performed for the spin texture in a degenerate  $F = 1$   $^{87}\text{Rb}$  spinor Bose gas and in a caesium Bose-Einstein condensate [20,21], we investigate the density-weighted magnetization correlator and the magnetization variance. These quantities

\*rosario@fisica.unam.mx

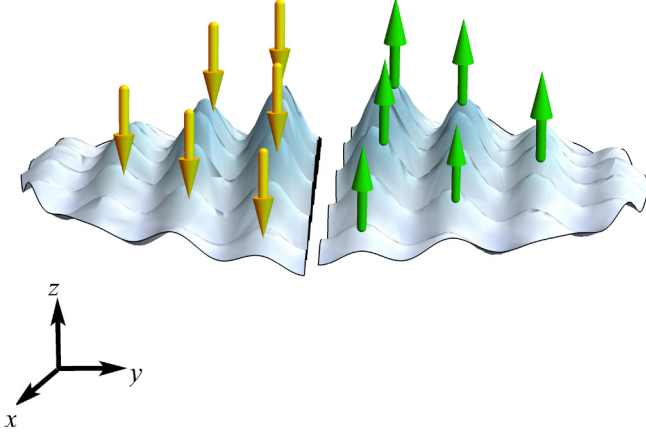


FIG. 1. Schematic form of the density profile prepared as the initial state. The left and right sides represent the superfluid density associated with the hyperfine components  $\uparrow$  and  $\downarrow$ . Such profiles correspond to densities at zero disorder amplitude and given values of the intra- and interspecies interactions amplitudes  $g_{\uparrow\uparrow} = g_{\downarrow\downarrow}$  and  $g_{\uparrow\downarrow}$ .

provide information about the magnetization anisotropy and the decaying of the magnetization as a function of time, respectively.

This work is organized as follows. In Sec. II, we present the model used to describe the dynamics of the initial ferromagnetic domains under the influence of disorder. We briefly explain the construction of the initial state from which the evolution in time is followed. In Sec. III A, we show the results of our numerical study concerning the dynamic extinction of ferromagnetic domains, as a function of the disorder amplitude and different interaction strengths. In Sec. III B, we analyze the behavior of the variance and spatial correlations, which allows us to follow the process of demagnetization in time and space. Finally, in Sec. IV, we summarize our findings.

## II. MODEL AND INITIAL STATE PREPARATION

We consider a weakly interacting mixture of two hyperfine spin components,  $|\uparrow\rangle = |F=1, m_F=-1\rangle$  and  $|\downarrow\rangle = |F=2, m_F=-2\rangle$ , of ultracold  $^{87}\text{Rb}$  atoms confined in an inhomogeneous disordered square lattice. At zero temperature and within the mean-field formalism, the wave functions  $\Psi_{\uparrow,\downarrow}$  of the two species  $\uparrow$  and  $\downarrow$  obey the following effective GP equations:

$$\begin{aligned} i\hbar \frac{\partial \Psi_{\uparrow}(\vec{r}, t)}{\partial t} &= [H_0(\vec{r}) + g_{\uparrow\uparrow}|\Psi_{\uparrow}|^2 + g_{\uparrow\downarrow}|\Psi_{\downarrow}|^2]\Psi_{\uparrow}(\vec{r}, t), \\ i\hbar \frac{\partial \Psi_{\downarrow}(\vec{r}, t)}{\partial t} &= [H_0(\vec{r}) + g_{\downarrow\downarrow}|\Psi_{\downarrow}|^2 + g_{\downarrow\uparrow}|\Psi_{\uparrow}|^2]\Psi_{\downarrow}(\vec{r}, t), \end{aligned} \quad (1)$$

where  $H_0(\vec{r}) = -\frac{\hbar^2}{2m}\nabla_{\perp}^2 + V_{\text{ext}}(\vec{r})$ , with  $\nabla_{\perp}^2 = \frac{\partial^2}{\partial x^2} + \frac{\partial^2}{\partial y^2}$  being the Laplacian operator in 2D and  $m$  the equal mass of the two spin components. The external potential has the following

form:

$$V_{\text{ext}}(\vec{r}) = \frac{1}{2}m\omega_r^2 r^2 + V_0^{\delta} \left[ \cos^2\left(\frac{\pi x}{a}\right) + \cos^2\left(\frac{\pi y}{a}\right) \right], \quad (2)$$

where  $\vec{r} = x\hat{i} + y\hat{j}$ ;  $\omega_r = 2\pi \times 50$  Hz is the radial harmonic frequency, fixed to a common value used in current experiments;  $a$  is the lattice constant; and  $V_0^{\delta} = V_0[1 + \epsilon_{\delta}(x, y)]$  is the potential depth at each point  $(x, y)$ . The function  $\epsilon_{\delta}(x, y)$  represents a random disorder uniformly distributed in the interval  $\epsilon_{\delta}(x, y) \in [-\delta, \delta]$ . Thus, the random depth  $V_0^{\delta}$  mimics a disordered environment like that introduced by speckle patterns [22]. The amplitude of  $V_0^{\delta}$  is scaled, as usual, in units of the recoil energy  $E_R = \frac{\hbar^2 k^2}{2m}$ , with  $k = \pi/a$ .

The interaction couplings  $g_{\sigma\sigma'} = 4\pi N\hbar^2 a_{\sigma\sigma'}/m$ , with  $\sigma\sigma' = \{\uparrow, \downarrow\}$ , are written, as usual, in terms of the  $s$ -wave scattering length  $a_{\sigma\sigma'}$ ,  $N$  being the number of atoms in the condensate. However, we should point out here that these interaction coefficients must be rescaled since the dynamics under study occurs in 2D [23–29]. The effective scattering length in the plane  $x$ - $y$  becomes  $a_{\sigma\sigma'} \rightarrow a_{\sigma\sigma'}/\sqrt{2\pi}l_z$ , with  $l_z = \sqrt{\hbar/m\omega_z}$ ,  $\omega_z$  being a common transverse frequency of condensates [30,31]. In typical experiments the values of the coupling constants  $g_{\sigma\sigma'}$  can be varied via Feshbach resonances and thus adjusted to have either equal or different values of the intra- and interspecies interactions, that is,  $g_{\uparrow\uparrow} = g_{\downarrow\downarrow} = g_{\uparrow\downarrow}$  or  $g_{\uparrow\uparrow} = g_{\downarrow\downarrow} \neq g_{\uparrow\downarrow}$ . In the present investigation we consider the interaction couplings  $g_{\uparrow\uparrow} = g_{\downarrow\downarrow}$  and  $g_{\uparrow\downarrow} = g_{\downarrow\uparrow}$  that ensure the miscibility of the hyperfine components  $g_{\uparrow\downarrow} < \sqrt{g_{\uparrow\uparrow}g_{\downarrow\downarrow}}$  [11,32].

### Initial ferromagnetic state

To create the initial state from which we follow the demagnetization process, we first determine the stationary states of the coupled equations (1) by means of the imaginary time evolution  $\tau \rightarrow i\tau$  [33–36] for a disorder-free optical lattice with the lattice spacing  $a = 532$  nm,  $N = 600$  atoms, and a potential depth of  $V_0/E_R = 4$  (see the Appendix). After free energy minimization, we manually remove  $\sigma = \uparrow$  particles from the left-half layer and  $\sigma = \downarrow$  particles from the right-half layer (see Fig. 1). This removal of particles mimics experimental protocols in which a digital mirror device is used to optically remove the atoms at specific positions [17]. Here, we perform the dismissing of particles in order to manually design a state that displays two ferromagnetic domains with opposite magnetization and equal hyperfine densities. Alternatively, another experimental and numerical route to achieve magnetic domains is through a magnetic field gradient [37].

## III. RESULTS AND DISCUSSION

In our simulations we consider lattices having  $\sim 30 \times 30$  occupied sites. As stated in Sec. II, the uncorrelated disorder is introduced across the whole lattice through the function  $\epsilon_{\delta}(x, y)$ . To perform a reliable analysis of the physical quantities and have meaningful predictions, we take the average over an ensemble of 200 realizations for each value of the disorder amplitude  $\delta$  and given values of the ratio between intra- and interspecies interactions  $g_{\uparrow\downarrow}/g_{\uparrow\uparrow}$ . We note that

the way in which the disorder has been simulated warrants that, although the lattice symmetry is altered, the underlying structure is preserved; that is, the square geometry and the harmonic confinement prevail. In the following, we identify the dimensionless time as  $\tau = E_{Rt}/\hbar$ .

The time propagation of the double ferromagnetic domain takes place after introducing the disordered potential and properly adjusting the interaction coefficients due to the removal of half the population,  $N \rightarrow N/2$ . This pattern created at hand, that is, the two ferromagnetic domains, is our starting point to study the time evolution under the influence of static uncorrelated disorder. We should note here that such an initial state is nonstationary and, consequently, evolves under its own dynamics. Interestingly, the protocol planned mimics a quantum quench process since a closed system left in an eigenstate of a given Hamiltonian at  $t = 0$  evolves dynamically under a different Hamiltonian. In Fig. 1 we show a schematic plot of the initial state. Our particular interest is to investigate how the local magnetization of the ferromagnetic domains degrades when the weakly interacting 2D Bose mixture evolves in the absence of other external fields, except for the one produced from the combination of a speckle pattern and the square lattice. To this end, in the subsections below we study both the magnetization as a function of time and the magnetization correlations in time and space.

### A. Demagnetization vs disorder: Magnetization dynamics

The observables to be studied in this section are the magnetization  $m_L$  and  $m_R$ , in the left and right sides of the lattice, as a function of time. These quantities are defined in terms of the local magnetization  $m(x, y; t) = \rho_{\uparrow}(x, y; t) - \rho_{\downarrow}(x, y; t)$ , where  $\rho_{\uparrow}(x, y; t)$  and  $\rho_{\downarrow}(x, y; t)$  are the densities associated with the components  $\uparrow$  and  $\downarrow$ , respectively. Thus, the magnetizations in the left and right sides are as follows:

$$\begin{aligned} m_L &= \iint_{\Omega_L} dx dy m(x, y; t), \\ m_R &= \iint_{\Omega_R} dx dy m(x, y; t), \end{aligned} \quad (3)$$

where  $\Omega_L$  and  $\Omega_R$  are the left and right halves of the system, respectively. Because of the particular election of the initial state we have that  $m_L(t = 0) = -0.5$  and  $m_R(t = 0) = 0.5$ . For our analysis, besides the set of random realizations  $\epsilon_{\delta}(x, y)$  for a given disorder magnitude, we consider three different values of the ratio  $g_{\uparrow\uparrow}/g_{\uparrow\downarrow}$ . The time dynamics is followed for a period of time such that at zero disorder and a given value of the coupling interactions the magnetization in the left and right sides become null. That is, the decay of magnetization at zero disorder is different for each ratio  $g_{\uparrow\downarrow}/g_{\uparrow\uparrow}$  considered. It is important to mention here that all of our numerical calculations were performed ensuring that changing  $\tau \rightarrow -\tau$  at any temporal step along the time dynamics allows us to recover the initial state.

Since the prepared initial state is nonstationary, the hyperfine spin populations will evolve under the influence of both disorder and interactions. Previous analyses of stationary properties in a single Bose-Einstein condensate component

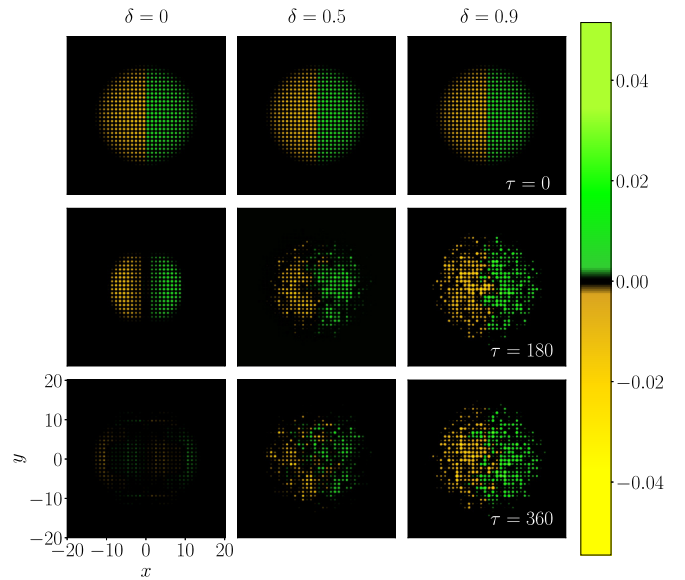


FIG. 2. Instantaneous density plots of the local magnetization  $m(x, y, \tau)$  in the square lattice for three different values of the disorder amplitude. Distance along  $x$  and  $y$  axis is scaled in terms of the lattice constant  $a$ . Left, center and right columns correspond to three different values of disorder amplitude  $\delta$  as indicated in the figure. Upper, middle and bottom rows are associated to  $\tau = 0$ ,  $\tau = 180$  and  $\tau = 360$  respectively. The ratio of the intra and inter-species interaction is,  $g_{\uparrow\downarrow} = 0.9g_{\uparrow\uparrow}$ .

confined in disordered lattices have shown that, in the weakly interacting regime, the net effect of the disorder is to localize the condensate density in bounded regions [19,38–41]. As a matter of fact, the size of those bounded regions becomes shorter and shorter as the amplitude of the disorder strength is increased. Therefore, what we expect in the case of the two-component condensate is to have spatially localized densities of the condensate as the disorder magnitude grows and thus preservation of magnetic domains.

In Fig. 2 we show snapshots of the local magnetization for three different values of the disorder amplitude,  $\delta = 0$ ,  $\delta = 0.5$ , and  $\delta = 0.9$  (left, center, and right columns, respectively), and three different times along the dynamics,  $\tau = 0$ ,  $\tau = 180$ , and  $\tau = 360$ . Each plot is a snapshot associated with a given realization of disorder  $\epsilon_{\delta}(x, y)$  and a fixed value of the intra- and interspecies interaction ratio,  $g_{\uparrow\downarrow}/g_{\uparrow\uparrow} = 0.9$ . As one can see from this figure, at zero disorder amplitude,  $\uparrow$  and  $\downarrow$  density configurations remain exactly opposite while showing an asymmetric behavior for  $\delta \neq 0$ . We also observe that larger values of the disorder amplitude lead to a slowdown of the dynamics of the magnetic domains. That is, the initial state remains for larger times, thus showing a persistence of the magnetic domains during the time evolution. Figure 2 is representative of the magnetization behavior observed at different times as the disorder is increased for the ensemble of disorder realizations.

In Fig. 3 we summarize the results of the analysis of this section. Each plot in this figure corresponds to the average of the magnetization on the right (left panels) and left (right panels) sides of the lattice as a function of time for different values of the disorder amplitude  $\delta$ . The specific values of  $\delta$

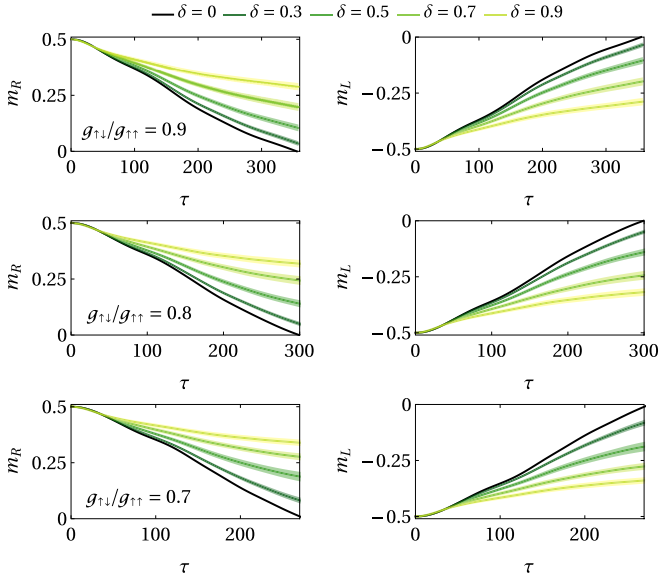


FIG. 3. Magnetization in right and left sides as a function of time for different values of disorder amplitude  $\delta$ . The ratio of the intra- and interspecies interaction  $g_{\uparrow\downarrow}/g_{\uparrow\uparrow}$  is indicated in the left panels. Each point in these curves is the result of the average over 200 realizations of disorder for a given value of  $\delta$ . The shadow area around each curve corresponds to the root-mean-square deviation.

as well as the intra- and interspecies interaction ratio  $g_{\uparrow\downarrow}/g_{\uparrow\uparrow}$  are indicated in the figures. The curves in each plot are the averages for a given value of  $\delta$ , with the shadow area around each curve indicating its root-mean-square deviation. From these figures one can observe that for short times,  $\tau \lesssim 50$ , the general behavior of the decreasing magnetization takes very similar values, independently of the disorder strength. However, for longer times,  $\tau \gtrsim 50$ , each magnetization curve departs from each other, thus revealing the effects of the disordered medium. Furthermore, as the disorder amplitude is increased, the ferromagnetic order in each domain is preserved against depletion. In particular, for the largest value of the disorder amplitude considered, that is,  $\delta = 0.9$ , the value of the magnetization in the left and right sides remains unaltered around 50%. One can also notice two main outcomes associated with the value of the ratio  $g_{\uparrow\downarrow}/g_{\uparrow\uparrow}$ . One is that at zero disorder the time at which the magnetization is annihilated decreases as the ratio  $g_{\uparrow\downarrow}/g_{\uparrow\uparrow}$  is diminished. In contrast, as this ratio is increased, the reduction of the magnetization becomes progressively worse with respect to its initial value.

The time dependence of the left and right magnetizations are well described by the power-law ansatz  $m_R(\tau) \propto b(\delta)\tau^{\gamma(\delta)}$ . We fit the curves of Fig. 3 with such a power-law ansatz at intermediate-time scales, where one neglects the transient behavior at short times. We should notice that the coefficients  $\gamma$  and  $b$  also depend upon the ratio between  $g_{\uparrow\downarrow}$  and  $g_{\uparrow\uparrow}$ . In Fig. 4 we plot the behavior of  $\gamma$  as a function of  $\delta$ . From this figure one can notice how the value of the characteristic exponent  $\gamma$  is modified as the ratio  $g_{\uparrow\downarrow}/g_{\uparrow\uparrow}$  is varied. Here it is important to stress that  $\gamma$  is also influenced by the presence of the harmonic confinement. The value of this exponent is reduced as  $\delta$  grows, and thus the magnetiza-

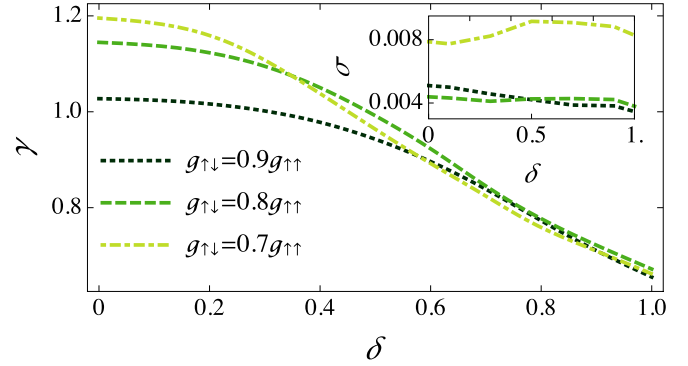


FIG. 4. Power-law fit  $m_R(\tau) \propto b(\delta)\tau^{\gamma(\delta)}$  for the magnetization on the right side as a function of  $\delta$ , for three different values of the ratio of the intra- and interspecies interaction. The inset shows the error  $\sigma$  of the magnetization fit.

tion extinction becomes slower in time. It is quite remarkable that for strong disorder strengths  $\delta$ , the parameters  $\gamma$  take very similar values, almost independent of the ratio of the inter- and intraspecies interaction coupling. This can indicate that the disorder has become the dominant contribution during the elapsed evolution. The inset in Fig. 4 shows the error of the magnetization fit.

#### B. Demagnetization vs disorder: Variance and magnetization correlator

Another suitable quantity that has been used in various experiments and provides crucial information on how magnetic domains change in space and time is the density-weighted magnetization correlator. As established in Refs. [20,21] this correlator is defined as

$$G(\Delta\vec{r}; t) = \frac{\int_{\Omega} m(\vec{r}; t)m(\vec{r} + \Delta\vec{r}; t)d\vec{r}}{\int_{\Omega} \rho(\vec{r}; t)\rho(\vec{r} + \Delta\vec{r}; t)d\vec{r}}, \quad (4)$$

where  $m(\vec{r}; t)$  is the local magnetization defined in the previous section,  $\rho(\vec{r}; t) = \rho_{\uparrow}(\vec{r}; t) + \rho_{\downarrow}(\vec{r}; t)$  is the total density, and  $\Omega = \Omega_L + \Omega_R$ . In Fig. 5 we illustrate the correlator  $G(\Delta\vec{r} = 0; t)$  for several values of the disorder strength and a fixed interaction ratio of  $g_{\uparrow\downarrow}/g_{\uparrow\uparrow} = 0.9$ . We should notice

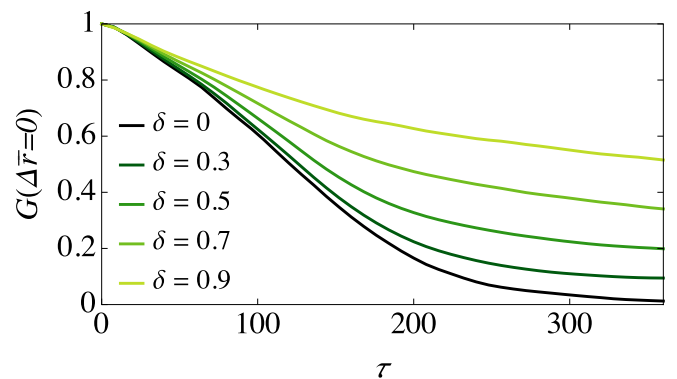


FIG. 5. Correlator  $G(\Delta\vec{r} = 0; \tau)$ , that is, variance as a function of time for different values of the disorder magnitude. Each curve is the average over 200 realizations of disorder  $\delta$ .



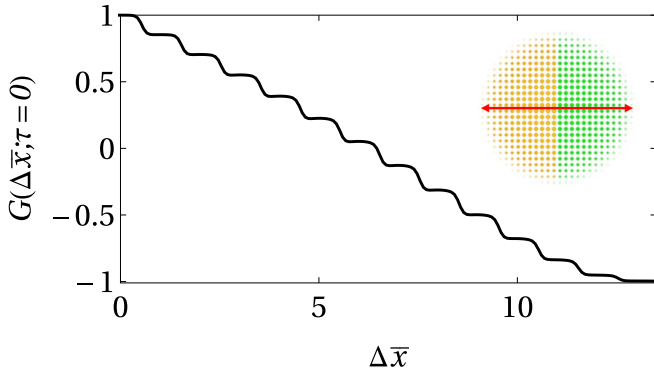


FIG. 6. Correlator  $G(\Delta\bar{x}; \tau)$  at  $\tau = 0$ . The inset shows the density profile prepared as the initial state. The red line shows the axis along which we determine the correlator  $G(\Delta\bar{x}; \tau)$ .

that for  $\Delta\vec{r} = 0$ , the density-weighted correlator coincides with the magnetization variance. For  $t = 0$ , the magnetization variance takes its largest value  $G(\Delta\vec{r} = 0; t = 0) = 1$  since the initial state corresponds to fully polarized domains. Then, for  $t > 0$  the variance shows a decreasing behavior in time, which becomes less pronounced as the disorder amplitude increases. As a matter of fact, for the largest value of the disorder amplitude considered, which is  $\delta = 0.9$  and at a time  $\tau = 360$ , the variance depletion is around half its initial value. In contrast, the magnetization variance becomes null at  $\tau = 360$  for zero disorder strength. Thus, one can appreciate that the structural disorder stimulates a deceleration of the polarization of the magnetic domains.

Since at  $t = 0$  down and up components lie on the left and right halves of a square lattice, a natural election of the path on which the spatial variations of the correlator  $G(\Delta\vec{r}; t)$  can be tracked is a line that crosses perpendicular to the halves of magnetic domains and then  $G(\Delta\vec{r}; t)$  becomes  $G(\Delta\bar{x}; t)$ . In Fig. 6 we illustrate both the axis in which the correlator is evaluated and its spatial variations for positive values of  $x$ . The staircase shape of the correlation function on Fig. 6 can be understood from the observation that the density at a given lattice site and in the region around it remains essentially constant.

To conclude the present analysis, in Fig. 7 we illustrate the spatial variations of the correlation function of Eq. (4) for  $\tau = 180$  and  $\tau = 360$ . As can be appreciated from Fig. 7 (upper panel), a depletion of the magnetic order is observed, since this reduction is less pronounced as the disorder decreases. Interestingly, all the curves get close when the correlation approaches zero, thus indicating that the domains still preserve information of the initial state. In contrast, the long-term dynamics illustrated in Fig. 7 (lower panel) shows higher discrepancies for each value of the disorder amplitude. In agreement with the previous findings, for  $\delta = 0$ , the magnetic order is completely lost. For the cases  $\delta = 0.3$  and  $\delta = 0.5$ , we observe residual domains that no longer conserve the initial structure. However, for  $\delta = 0.7$  and  $\delta = 0.9$ , the initial magnetic structure stands, with the polarization of the magnetic domains being reduced.

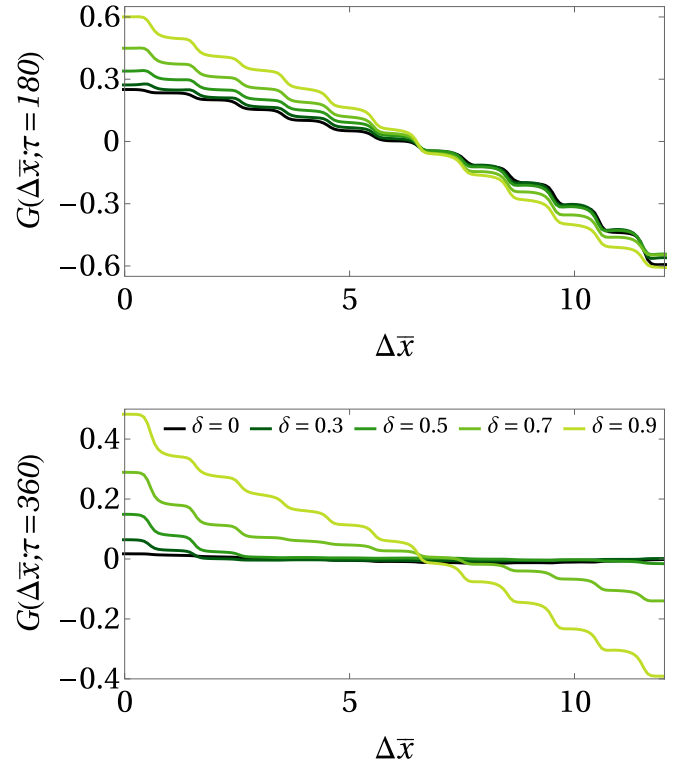


FIG. 7. Correlator  $G(\Delta\bar{x}; \tau_i)$  along the  $x$  axis for different values of the disorder magnitude. The upper and lower panels correspond to  $\tau = 180$  and  $\tau = 360$ , respectively. Each curve is the average over 200 realizations of disorder  $\delta$ .

#### IV. FINAL REMARKS

We have studied the time dynamics of initially localized ferromagnetic domains evolving under the influence of both disordered confinement and contact interactions. The purpose of such an investigation was to establish the persistence of ferromagnetic order in the domains, namely, spatial regions with definite magnetization, when the competition of structural disorder and interactions could lead the system, evolving under their inner dynamics, to nullify such an initial magnetic pattern. To study such a magnetization annihilation process as a function of time, we proposed a model system simulating a double ferromagnetic domain evolving under static disorder. The model consisted of a two-species  $^{87}\text{Rb}$  Bose-Einstein condensate, whose components labeled as  $\uparrow$  and  $\downarrow$  states were placed spatially separated, lying each one in the halves of a 2D potential resulting from the superposition of a harmonic potential and a square lattice. The description of the dynamics was addressed within the mean-field Gross-Pitaevskii approach by solving the coupled equations associated with different hyperfine components. To have a reliable analysis of the evolution in time of the magnetization under the presence of disorder, our analysis consisted of an extensive set of numerical calculations over different realizations of uncorrelated disorder having a given amplitude  $\delta$  and constant values of the intra- and interspecies interactions  $g_{\uparrow\downarrow}$  and  $g_{\uparrow\uparrow}$ , respectively. Regarding the magnitude of the intra- and interspecies interactions  $g_{\uparrow\downarrow}$  and  $g_{\uparrow\uparrow}$ , we worked in the regime in which the ratio between these coefficients  $g_{\uparrow\downarrow}/g_{\uparrow\uparrow}$

TABLE I. Physical parameters used in the numerical simulation.

Name	Symbol	Value
Particle number	$N$	600
$^{87}\text{Rb}$ mass	$m$	87 amu
Lattice constant	$a$	532 nm
Trap frequency ( $x$ )	$\omega_x$	$2\pi \times 50$ rad/s
Trap frequency ( $y$ )	$\omega_y$	$2\pi \times 50$ rad/s
Trap frequency ( $z$ )	$\omega_z$	$2\pi \times 4000$ rad/s
Bare $s$ -wave scattering length	$a_{\uparrow\uparrow} = a_{\downarrow\downarrow}$	$100 a_0$
Potential depth	$V_0$	$4 E_R$

guarantees miscibility of hyperfine components, and we also considered appropriate coupling interaction strengths away from the strong interaction effects. Besides the study of the dynamics of the magnetization in the presence of disorder, we analyzed the variance and the density-weighted magnetization correlator to investigate time and spatial magnetization decay, respectively.

The conclusion from the study of the magnetization dynamics is that the degradation of the initial double ferromagnetic domain, which is the loss of magnetization in definite regions of space, becomes slower and slower as the structural disorder is increased, while in contrast increasing the ratio between inter- and intraparticle contact interactions  $g_{\uparrow\downarrow}/g_{\uparrow\uparrow}$  tends to degrade the initial state. Furthermore, the analysis for the density-weighted correlator as a function of time and space reveals also such a persistence of the initial state as the disorder is increased. We reach these results from a robust study of the time evolution of the right and left magnetizations of the quantum system described above. Summarizing, our study allowed us to recognize that the slow extinction of the ferromagnetic order is induced by disorder and then enhancing memorylike effects in the coupled magnetic domains.

This paper sets a platform for the design of specific protocols appropriate to study demagnetization processes or frustration effects associated with geometry and energy disorder [42–45]. Also, our study aims for the investigation of the dynamics induced by measurement in the sense that sources of disorder can be either internal, like those here considered, or external, like those associated with reservoirs in contact with assessable quantum systems [46]. Textures or local magnetization, as referred to in the current literature, are suitable observables to track the effects of the disorder media in systems having more than one component and, also, are accessible physical quantities with single-spin-resolution techniques [47,48] used in current experimental setups. We expect that our work will trigger further theoretical analysis of, for instance, the long-range character proper of the dipole-dipole magnetic interactions and the homogeneous environ-

ment where the elemental constituents move. Those aspects still remain as open questions to be addressed. Understanding the dynamics of magnetic domains has become nowadays a relevant topic not only within the context of the fundamental physics but also associated with the emergence of technological uses. Practical applications of the investigation here presented are directly related to the design of magnetic logic and memory devices.

## ACKNOWLEDGMENTS

This work was partially funded by Grant No. IN108620 DGAPA (UNAM). G.A.D.-C., would like to thank V. Romero-Rochín for computational resources at Skymion IF-UNAM and R. Zamora-Zamora for useful guidance. G.A.D.-C., L.A.G.-G. and C.M. acknowledge scholarship from CONACYT.

## APPENDIX : NUMERICAL CALCULATIONS DETAILS

In this Appendix we provide additional details related to the numerical simulations performed in order to obtain the main results of the paper. As stated in Sec. II, we first obtain the ground state of the coupled GP equation shown in Eq. (1). This was achieved by using the imaginary-time propagation based on the split-step Fourier method [33,34]. The relevant physical parameters used in the simulations are included in Table I.

After accomplishing convergence of the ground-state wave functions, we performed the removal of particles by manually setting  $\Psi_{\uparrow} = 0$  in the left halve of the system  $\Omega_L$ . Analogously, we fixed  $\Psi_{\downarrow} = 0$  within the right halve  $\Omega_R$ . For simplicity, we normalized the resulting wave functions after the removal of particles.

The above procedure yields the initial configuration of the wave functions from which the demagnetization process was followed. The real-time dynamics was performed by using the fourth-order Runge-Kutta method. The numerical parameters used in both, the imaginary-time propagation and the real-time propagation, are shown in Table II.

TABLE II. Parameters for the numerical simulation.

Name	Symbol	Value
Number of grid points in the $x$ direction	$N_x$	512
Number of grid points in the $y$ direction	$N_y$	512
Spatial extension of the numerical grid in the $x$ direction	$L_x$	$40 a$
Spatial extension of the numerical grid in the $y$ direction	$L_y$	$40 a$
Step size used in real-time evolution	$d\tau$	0.001

- [1] F. J. Himpsel, J. E. Ortega, G. J. Mankey, and R. F. Willis, *Adv. Phys.* **47**, 511 (1998).  
 [2] Y. M. Kim, S. H. Han, H. J. Kim, D. Choi, K. H. Kim, and J. Kim, *J. Appl. Phys.* **91**, 8462 (2002).

- [3] T. Thomson, in *Metallic Films for Electronic, Optical and Magnetic Applications: Structure, Processing and Properties*, edited by K. Barmak and K. Coffey (Woodhead, Cambridge, England, 2014), p. 454.

- [4] A. Thiaville, Y. Nakatani, J. Miltat, and N. Vernier, *J. Appl. Phys.* **95**, 7049 (2004).
- [5] K. J. A. Franke, B. Van de Wiele, Y. Shirahata, S. J. Hämäläinen, T. Taniyama, and S. van Dijken, *Phys. Rev. X* **5**, 011010 (2015).
- [6] C. J. Myatt, E. A. Burt, R. W. Ghrist, E. A. Cornell, and C. E. Wieman, *Phys. Rev. Lett.* **78**, 586 (1997).
- [7] G. Modugno, M. Modugno, F. Riboli, G. Roati, and M. Inguscio, *Phys. Rev. Lett.* **89**, 190404 (2002).
- [8] G. Thalhammer, G. Barontini, L. De Sarlo, J. Catani, F. Minardi, and M. Inguscio, *Phys. Rev. Lett.* **100**, 210402 (2008).
- [9] A. D. Lercher, T. Takekoshi, M. Debatin, B. Schuster, R. Rameshan, F. Ferlaino, R. Grimm, and H.-C. Nägerl, *Eur. Phys. J. D* **65**, 3 (2011).
- [10] D. J. McCarron, H. W. Cho, D. L. Jenkin, M. P. Köppinger, and S. L. Cornish, *Phys. Rev. A* **84**, 011603(R) (2011).
- [11] F. Wang, X. Li, D. Xiong, and D. Wang, *J. Phys. B: At. Mol. Opt. Phys.* **49**, 015302 (2016).
- [12] E. A. Hinds and I. G. Hughes, *J. Phys. D: Appl. Phys.* **32**, R119 (1999).
- [13] R. Grimm, M. Weidemüller, and Y. B. Ovchinnikov, *Adv. At., Mol., Opt. Phys.* **42**, 95 (2000).
- [14] M. Lewenstein, A. Sanpera, V. Ahufinger, B. Damski, A. Sen, and U. Sen, *Adv. Phys.* **56**, 243 (2007).
- [15] C. Gross and I. Bloch, *Science* **357**, 995 (2017).
- [16] A. L. La Rooij, H. B. van Linden van den Heuvell, and R. J. C. Spreeuw, *Phys. Rev. A* **99**, 022303 (2019).
- [17] J.-Y. Choi, S. Hild, J. Zeiher, P. Schauß, A. Rubio-Abadal, T. Yefsah, V. Khemani, D. A. Huse, I. Bloch, and C. Gross, *Science* **352**, 1547 (2016).
- [18] A. Rubio-Abadal, J.-y. Choi, J. Zeiher, S. Hollerith, J. Rui, I. Bloch, and C. Gross, *Phys. Rev. X* **9**, 041014 (2019).
- [19] L. A. González-García, S. F. Caballero-Benítez, and R. Paredes, *Sci. Rep.* **9**, 11049 (2019).
- [20] J. Guzman, G.-B. Jo, A. N. Wenz, K. W. Murch, C. K. Thomas, and D. M. Stamper-Kurn, *Phys. Rev. A* **84**, 063625 (2011).
- [21] C. V. Parker, L.-C. Ha, and C. Chin, *Nat. Phys.* **9**, 769 (2013).
- [22] P. Bouyer, *Rep. Prog. Phys.* **73**, 062401 (2006).
- [23] A. Posazhennikova, *Rev. Mod. Phys.* **78**, 1111 (2006).
- [24] L. Salasnich, A. Parola, and L. Reatto, *Phys. Rev. A* **65**, 043614 (2002).
- [25] A. Muñoz Mateo and V. Delgado, *Phys. Rev. A* **77**, 013617 (2008).
- [26] W. Bao, D. Jaksch, and P. A. Markowich, *J. Comput. Phys.* **187**, 318 (2003).
- [27] C. Trallero-Giner, R. Cipolatti, and T. C. H. Liew, *Eur. Phys. J. D.* **67**, 143 (2013).
- [28] R. Zamora-Zamora R, G. A. Domínguez-Castro, C. Trallero-Giner, R. Paredes, and V. Romero-Rochín, *J. Phys. Commun.* **3**, 085003 (2019).
- [29] D. S. Petrov, M. Holzmann and G. V. Shlyapnikov, *Phys. Rev. Lett.* **84**, 2551 (2000).
- [30] Z. Hadzibabic, P. Krüger, M. Cheneau, B. Battelier, and J. Dalibard, *Nature (London)* **441**, 1118 (2006).
- [31] C.-L. Hung, X. Zhang, N. Gemelke, and C. Chin, *Nature (London)* **470**, 236 (2011).
- [32] S. B. Papp, J. M. Pino, and C. E. Wieman, *Phys. Rev. Lett.* **101**, 040402 (2008).
- [33] P. Muruganandam and S. K. Adhikari, *Comput. Phys. Commun.* **180**, 1888 (2009).
- [34] D. Vudragović, I. Vidanović, A. Balaž, P. Muruganandam, and S. K. Adhikari, *Comput. Phys. Commun.* **183**, 2021 (2012).
- [35] R. Dum and Y. Castin, *Eur. Phys. J. D* **7**, 399 (1999).
- [36] R. Zeng and Y. Zhang, *Comput. Phys. Commun.* **180**, 854 (2008).
- [37] D. M. Weld, P. Medley, H. Miyake, D. Hucul, D. E. Pritchard, and W. Ketterle, *Phys. Rev. Lett.* **103**, 245301 (2009).
- [38] S. Ray, M. Pandey, A. Ghosh, and S. Sinha, *New. J. Phys.* **18**, 013013 (2016).
- [39] T. Schulte, S. Drenkelforth, J. Kruse, R. Tiemeyer, K. Sacha, J. Zakrzewski, M. Lewenstein, W. Ertmer, and J. J. Arlt, *New. J. Phys.* **8**, 230 (2006).
- [40] S. K. Adhikari and L. Salasnich, *Phys. Rev. A* **80**, 023606 (2009).
- [41] M. Kobayashi, M. Tsubota, and T. Iida, *Physica B (Amsterdam, Neth.)* **329–333**, 210 (2003).
- [42] M. S. Pierce, C. R. Buechler, L. B. Sorensen, S. D. Kevan, E. A. Jagla, J. M. Deutsch, T. Mai, O. Narayan, J. E. Davies, K. Liu, G. T. Zimanyi, H. G. Katzgraber, O. Hellwig, E. E. Fullerton, P. Fischer, and J. B. Kortright, *Phys. Rev. B* **75**, 144406 (2007).
- [43] Y. W. Windsor, A. Gerber, and M. Karpovski, *Phys. Rev. B* **85**, 064409 (2012).
- [44] I. Korzhovska, H. Deng, L. Zhao, Z. Chen, M. Konczykowski, S. Zhao, S. Raoux, and L. Krusin-Elbaum, *npj Quantum Mater.* **5**, 39 (2020).
- [45] J. Reindl, H. Volker, N. P. Breznay, and M. Wuttig, *npj Quantum Mater.* **4**, 57 (2019).
- [46] H. M. Hurst and I. B. Spielman, *Phys. Rev. A* **99**, 053612 (2019).
- [47] C. Weitenberg, M. Endres, J. F. Sherson, M. Cheneau, P. Schauß, T. Fukuhara, I. Bloch, and S. Kuhr, *Nature (London)* **471**, 319 (2011).
- [48] M. Boll, T. A. Hilker, G. Salomon, A. Omran, J. Nespolo, L. Pollet, I. Bloch, and C. Gross, *Science* **353**, 1257 (2016).